Special Issue Article

Advances in Mechanical Engineering

Advances in Mechanical Engineering
2016, Vol. 8(6) 1–11

DOI: 10.1177/1687814016651557
aime.sagepub.com
SAGE

Simulation of rock fragmentation induced by a tunnel boring machine disk cutter

Huiyun Li[1,2] and Erxia Du[2]

Abstract

A constitutive model based on the Johnson–Cook material model and the extended Drucker–Prager strength criterion was implemented in LS-DYNA to simulate the rock failure process induced by a single disk cutter of a tunnel boring machine. The normal, rolling, and side forces were determined by numerical tests. The simulation results showed that the normal and rolling forces increased with increasing penetration while the side force changed little. The normal force also increased under the conditions of confining pressures. The damage region of rock and cutting forces were also obtained by simulation of two disk cutters acting in tandem with different cutting spacings. The optimum ratio of cutter spacing to penetration depth determined from numerical modeling agrees well with that obtained by linear cutting machine tests. The average normal and rolling forces acting on the first cutter are slightly greater than those acting on the second when the cutting disk spacing is relatively small. The numerical modeling was verified to accurately capture the fragmentation of rock induced by disk cutter.

Keywords

Tunnel boring machine disk cutter, rock, material model, cutting force, fragmentation

Date received: 28 September 2015; accepted: 5 April 2016

Academic Editor: António Mendes Lopes

Introduction

Tunnel boring machines (TBMs) have been widely used in tunnel construction for a variety of purposes such as highways and subways. The cutter-head design is one of the critical aspects of the TBM manufacturing process. The head diameter, number of cutters, thrust force, rolling force, penetration depth, and cutter spacing are the important parameters in head design. Among these, the cutting forces and appropriate cutter spacing are the main factors governing cutting efficiency.[1] Disk cutters are the main tools employed by TBMs for fragmenting rock. However, this essential component is easily worn. It is, therefore, necessary to analyze the cutting forces acting on a disk cutter and determine its failure mechanisms for better TBM head design and improved cutting efficiency.

For determination of the forces acting on TBM disk cutters and for establishing optimum cutting settings, full-scale linear cutting machine (LCM) test has been proved to be a reliable method.[2–5] Although full-scale tests have significant advantages, they are expensive and time-consuming.[1] To overcome these deficiencies, well-known prediction models, for example, Colorado School of Mines (CSM)[6] and Norwegian University of

[1]Department of Mechanics, School of Mechanical Engineering, Tianjin University, Tianjin, China
[2]School of Civil Engineering, Hebei University, Baoding, China

Corresponding author:
Huiyun Li, Department of Mechanics, School of Mechanical Engineering, Tianjin University, Tianjin 300072, China.
Email: li_huiyun1977@126.com

Science and Technology (NTNU),[7] have been developed to predict the performance of TBMs. Numerous examples of theoretical and semi-theoretical formulas can be found in the literature.[8–13] However, these simple analytical models can provide only an approximate estimation of the cutting forces. Barton[14] introduced a predictive formulation of TBM performance using the rock mass quality index (Q_{TBM}). Rock mass classification systems such as the Q-system and rock mass rating (RMR) system have also been used for the estimation of TBM performance.[15] Zhao et al.[16] established a prediction model of TBM performance using ensemble neural network analysis for granitic rock masses. Empirical prediction models are mainly established according to experience and previously recorded data in the field. The accuracy and reliability of these models depend on the quality and amount of the data available. It is generally difficult to collect substantial amounts of high-quality data.

Numerous researchers have applied numerical modeling to simulate the fragmentation of rock by TBMs. The prediction of the fragmentation process during rock cutting using various numerical methods was reviewed in detail by Menezes et al.[17] Most studies have focused on the modeling of linear slab cutting due to its simplicity. Several methods have been used to simulate the cutting process such as the finite differential method (FDM), displacement discontinuity method (DDM), discrete element method (DEM), and finite element method (FEM). For example, the FLAC program employs an explicit FDM for computational engineering mechanics applications. Park et al.[18] developed a heterogeneous two-dimensional (2D) model using FLAC to evaluate the effect of confining pressure and cutter spacing on the fragmentation of rock. Innaurato et al.[19] studied the rock fracture and chipping formation of a TBM disk cutter. The authors used Mohr–Coulomb material constitutive model for the rock. Tulu and Heasley[20] adopted the commercial three-dimensional (3D) FDM code FLAC3D to simulate circular groove cutting. A rock indentation model was developed by Tan et al.,[21] in which a modified energy criterion was incorporated into a DDM code. DEM and FEM are, however, the most widely used numerical methods for rock-cutting analysis. In fact, of these two, the FEM is clearly the most commonly employed numerical method for all engineering sciences, including rock mechanics and rock engineering.[22] Gong et al.[23–26] explored the effect of joint spacing and orientation on rock fragmentation using universal distinct element code (UDEC) based on a 2D DEM. DEM has also been used by Rojek et al.[27,28] for the simulation of rock-cutting processes. Moon and Oh[29] employed the commercial 2D DEM code PFC^{2D} to simulate the optimal rock-cutting phenomena according to the ratio of the cutter spacing to the penetration depth (s/p) using the properties of intact rock. Su and Akcin[30] and Mendoza Rizo[31] employed the 3D DEM code PFC^{3D} to predict cutter forces from cutting tests. Huang et al.[32,33] employed a DEM to study the failure mechanisms induced by a wedge-shaped tool indenting normally against a rock surface. Tang[34] developed a numerical approach denoted as rock failure process analysis (RFPA) based on FEM. Tang et al.[35] simulated the fracture of rock containing grains or inclusions using RFPA. Liu et al.[36] simulated rock cutting with the FEM code $R\text{-}T^{2D}$ to evaluate the rock fragmentation process induced by single and double indenters. Cho et al.[1] employed FEM with explicit time integration software AUTODYN-3D to simulate the failure process of rock observed during LCM test. Yu[37] employed LS-DYNA software to simulate the rotation of a continuous miner cutter head while cutting rock. Jaime[38] reproduced the failure mode in linear cutting using LS-DYNA software and successfully modeled the crushing failure mode in shallow cutting and the crack initialization, crack propagation, and dynamic fragmentation in deep cutting.

While the DEM and FEM are most commonly employed for modeling rock-cutting process, they have their individual strengths and weaknesses. Although the DEM is able to model the majority of primary rock-cutting phenomena, the material model must be built at the micro-level. However, the FEM employing continuum damage models is able to model both the ductile and brittle damage modes. Hence, this method was adopted for this study. The FEM can also provide detailed information on the distribution of stresses, strains, and strain rates in the chip formation zone. This detailed information cannot be easily obtained using other methods such as analytical and experimental or empirical methods.[17] This study employed the explicit FEM code LS-DYNA, which is capable of capturing dynamic interactions during rock cutting.

The rock-cutting process is a complex dynamic process with complicated nonlinear characteristic, and the numerical modeling of the process requires a detailed constitutive material model for rock that can account for the complicated behavior of rock under various conditions of stress. The strength of rock is usually a function of pressure, strain rate, temperature, and damage. Various models have been used such as the elastic, von Mises, Mohr–Coulomb, Drucker–Prager, and Hoek–Brown models. The Mohr–Coulomb and Drucker–Prager failure criterion have typically been utilized for modeling rock materials in the numerical simulation of the rock-cutting process, although they considered only the influence of static stress. The effects of high confining pressure and strain rate and temperature on rock strength are not considered. This article presents a rock damage material model based on the Johnson–Cook material model[39] and extended

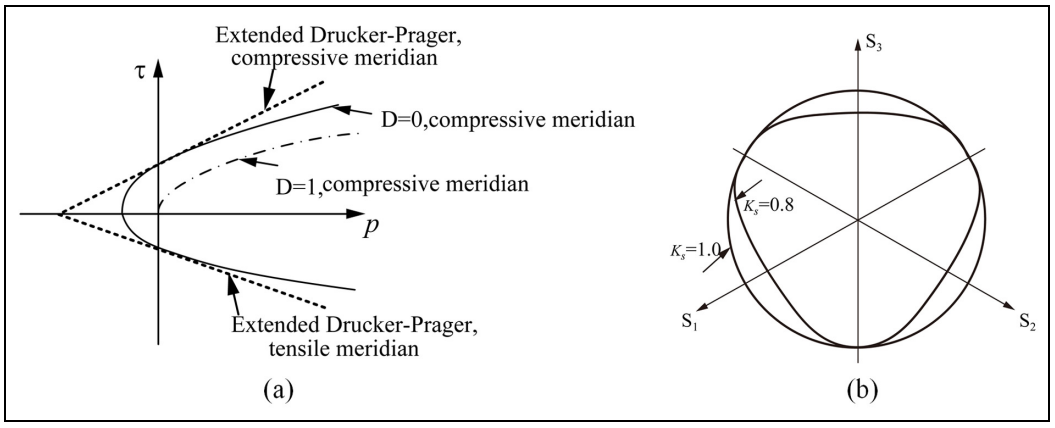

Figure 1. Failure criterion adopted in the material model: (a) in the meridian plane and (b) in the deviatoric plane.[40]

Drucker–Prager strength criterion,[40] which considers temperature, confining pressures, and strain rates. The damage model is applied to analyze the rock damage induced by TBM disk cutters.

Material constitutive model for rock

The selection of constitutive models for rock failure plays an important role in rock mechanics and rock engineering, especially in the fields of numerical modeling.[38] The compressive strength of rock is increased with increasing lateral confining pressure and strain rate and decreased with increasing temperature. A reliable computational material model for rock should include features such as the combined hardening of the strain rate and pressure, the softening effect of high temperature. This article presents a rock material model that considers confining pressures and strain rates and temperature, based on the Johnson–Cook model[39] and extended Drucker–Prager strength criterion.[40]

The yield surface of rock can be expressed as a function of hydrostatic pressure, strain rate, temperature, and damage. The specific expression is

$$\frac{\tau}{f_c} = \left[A(1-D) + B(p^*)^N\right]\left[1 + C\ln(\dot{\varepsilon}^*)\right]\left[1 - \left(T^*_{tem}\right)^M\right] \tag{1}$$

where $\tau = (1/2)\sigma_{eq}[1 + (1/Ks) - (1 - (1/Ks))(r/\sigma_{eq})^3]$; $\sigma_{eq} = \sqrt{3J_2} = \sqrt{(3/2)s_{ij}s_{ij}}$; $r^3 = (9/2)s_{ij}s_{jk}s_{kj} = (27/2)J_3$; s_{ij} is the stress deviator; and J_2 and J_3 are the second and third invariants of the deviatoric stress tensor, respectively; f_c is the quasi-static uniaxial compressive strength; D is the compressive damage parameter; $p^* = p/f_c$ is the normalized pressure (p is the actual pressure); $\dot{\varepsilon}^* = \dot{\varepsilon}/\dot{\varepsilon}_0$ is the dimensionless strain rate; $T^*_{tem} = (T_c - T_r)/T_m - T_r$; T_c is the current temperature; T_r is a reference temperature (room temperature); and T_m is the melting temperature. Additionally, A, B, N, C, M, and Ks denote the material parameters, where A is the normalized cohesive strength, B is the normalized pressure hardening coefficient, N is the pressure hardening exponent, C is the strain rate coefficient, M is the temperature softening exponent, and Ks is the shape parameter of the yield surface in the deviatoric plane.

The deviatoric stress measure τ accounts for different responses under tension and compression through the parameter Ks, which varies in the range of $0.778 \leq Ks \leq 1.0$ to ensure the convexity of the yield surface. When $Ks = 1$, the dependence on the third deviatoric stress invariant is removed, and the original Drucker–Prager model is recovered.[40] The loading surface given by equation (1) is depicted in Figure 1.

The hydrostatic pressure is calculated by the equation of state, which has identical form with the original article of Holmquist et al.[41] The equation of state defines the hydrostatic pressure–volume relationship. The volumetric strain can be expressed in terms of the principal strain ε_{ii} as

$$\mu = \frac{V - V_0}{V_0} = (1+\varepsilon_{11})(1+\varepsilon_{22})(1+\varepsilon_{33}) - 1 \approx \varepsilon_{11} + \varepsilon_{22} + \varepsilon_{33} \tag{2}$$

where V_0 and V are the initial and current volumes. Under the action of high hydrostatic pressure, the pressure–volumetric strain response of rocks, respectively, can be divided into three regions as illustrated in Figure 2,[41] in which p_{crush} and μ_{crush} stand for, respectively, the pressure and volumetric strain value that occur in a uniaxial compression test; p_{lock} and μ_{lock} stand for the pressure and volumetric strain of the material compaction point.

The nonassociative plastic flow rule is used to describe the plastic strain rates. The plastic potential g is expressed as

$$g = \sqrt{3J_2} \tag{3}$$

Table 1. Parameters for Colorado red granite used in the numerical analyses.

ρ (kg/m^3)	E (GPa)	G (GPa)	ν	K (GPa)	A	B	C	N
2600	41	16.61	0.234	25.69	0.3	2.04	0.007	0.7
M	f_c (MPa)	f_t (MPa)	ε_0	EFMIN	p_{crush} (GPa)	μ_{crush}	p_{lock} (GPa)	μ_{lock}
1.5	158	6.78	1	0.01	0.0527	0.002	0.8	0.1
D_1	D_2	K_1 (GPa)	K_2 (GPa)	K_3 (GPa)	K_s	T (°C)	T_r (°C)	T_m (°C)
0.04	1	85	−171	208	0.8	20	20	1200

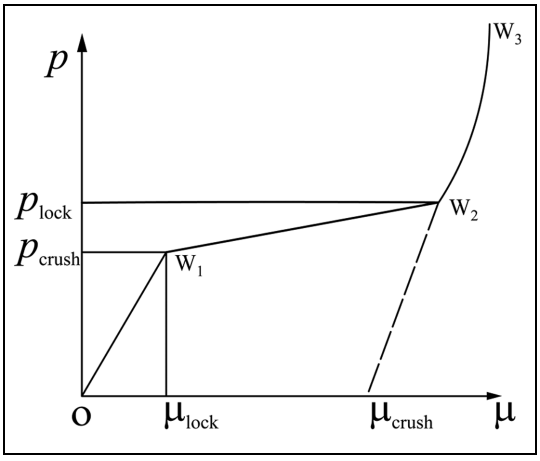

Figure 2. Relation of pressure and volumetric strain.

The rate of plastic strain is given as follows

$$d\varepsilon_{ij}^{p} = \dot{\lambda}\frac{\partial g}{\partial \sigma_{ij}} \tag{4}$$

where $\dot{\lambda}$ is the plastic multiplier.

The damage from fracture is accumulated in a manner similar to that used in the original Holmquist–Johnson–Cook (HJC) model.[41] The damage accumulating from equivalent plastic strain and plastic volumetric strain is expressed by the compressive damage parameter

$$D = \sum \frac{\Delta\varepsilon_{eff}^{p} + \Delta\mu_p}{\varepsilon_p^f + \mu_p^f} \tag{5}$$

where $\Delta\varepsilon_{eff}^{p}$ and $\Delta\mu_p$ are the equivalent plastic strain and plastic volumetric strain, respectively, and $\varepsilon_p^f + \mu_p^f = f(P)$ is the plastic strain to fracture under a constant pressure p. The expression is

$$\varepsilon_p^f + \mu_p^f = D_1(p^* + T^*)^{D_2} \geq \varepsilon_{f\min} \tag{6}$$

where D_1 and D_2 are constants; p^* is as defined previously; the normalized maximum tensile hydrostatic pressure is $T^* = f_t/f_c$, where f_t is the uniaxial tensile strength; and $\varepsilon_{f\min}$ is provided to allow for a finite amount of plastic strain to fracture the material.

Numerical simulation results and analysis

We used the 3D FEM numerical code LS-DYNA to simulate the rock failure process induced by disk cutter, which is capable of simulating nonlinear and dynamic fracture failures. The rock material model presented in the previous section was implemented in LS-DYNA via the user subroutine UMAT.

Single disk cutter rock fragmentation process

Finite element model of the rock and disk cutter system. In the numerical simulation process, the parameters for Colorado red granite with uniaxial compression strength of 158 MPa were used,[4] based on the material model described in section "Material constitutive model for rock." The material parameters are listed in Table 1. The size of the modeled rock specimen was 900 mm × 180 mm × 1700 mm.

A V-shaped cutting disk 432 mm (17 in) in diameter and 80 mm in thickness was modeled in the simulation. The dimensions of the disk cutter are illustrated in Figure 3. Disk cutters are generally made of high-strength steel, and the elastic modulus is much higher than that of rock. Therefore, the wear and deformation of the cutter can be neglected, and a rigid material model is applied to describe the disk cutter. The main parameters employed for the disk cutter are density = 8000 kg/m^3, Young's modulus = 210 GPa, and Poisson's ratio = 0.25.

Hexahedron eight-node elements (denoted as solid 164) were employed to model the rock and disk cutter system, where the finite element model is shown in Figure 4. The entire cutter body was represented by a ring configuration to reduce the number of elements required and therefore reduce the computational time. The Lagrange coordinate system was employed for the system. For the rock model, fixed restraints were applied to the bottom nodes of the simulated rock volume, and nonreflective boundaries on the surrounding

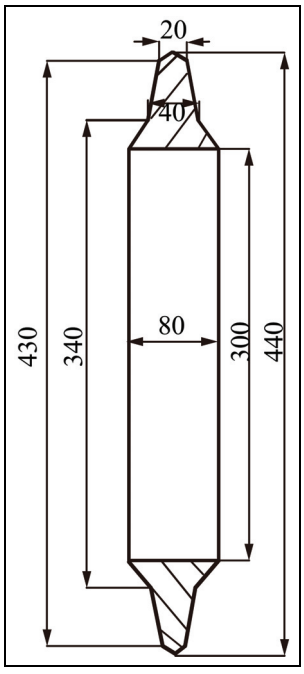

Figure 3. Dimensions (in mm) of the simulated disk cutter.

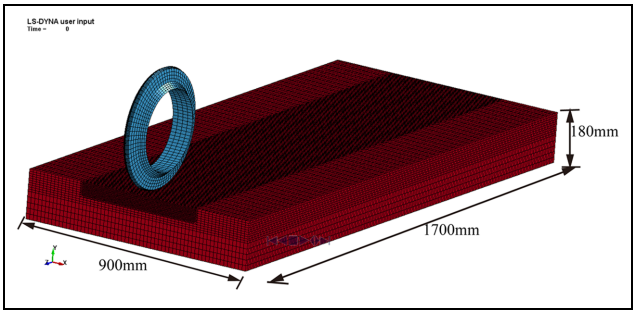

Figure 4. Finite element model of the rock and disk cutter.

surfaces of the rock were used to represent an infinite structure. For the disk cutter, linear displacement along the x-axis and the angular displacements about the y- and z-axes were restricted. The eroding surface-to-surface contact interface algorithm was adopted. The Flanagan–Belytschko stiffness, based on hourglass control, was applied for the rock elements. In this work, the strain failure criterion was used as an element erosion criterion. In LS-DYNA, all loadings must be defined as a function of time, and Table 2 lists the loading conditions acting on the disk cutter at different times. The total simulated time was for four seconds, and a total of 50 steps were exported 50 steps as results.

Simulation results and discussion. Figure 5 shows a schematic illustration of the main forces acting on a disk cutter, which are the normal force F_N, the rolling force F_R, and the side force F_S. F_N is used to calculate the overall thrust force of the TBM. F_R is used to calculate the torque and power requirements, as well as the specific energy (SE) of an excavator, given as the energy required to cut through a unit volume of rock. F_S is used to balance the cutter-head design.[42]

Table 2. Variation of loading with time for a constant angular velocity of −1.5 rad/s.

Time (s)	0	2	4
Penetration (mm)	0	−7.6	−7.6
Rolling displacement (mm)	0	−660	−1320
Angular velocity (mm)	−1.5	−1.5	−1.5

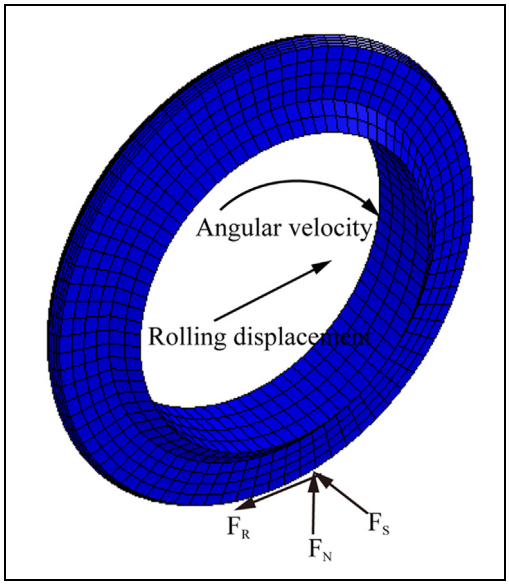

Figure 5. Normal force F_N, the rolling force F_R, and the side force F_S acting on a disk cutter rotating with some angular velocity, resulting in some rolling displacement.

The various forces acting on the cutter with respect to time are shown in Figure 6. The damage region of the simulated rock sample and its cross section normal to the z-axis are shown in Figure 7. As can be seen from the simulation results, the rock sample initially experienced elastic deformation. With increasing cutting forces and penetration depth, plastic deformation was produced as the compressive stress exceeded the uniaxial compression strength. The damage appeared with the accumulation of plastic deformation, and a crushed zone under the disk cutter was formed. F_N and F_R gradually increased during this stage. The deformation of rock increased with increasing penetration depth, and simulation elements were removed from the simulation whenever the erosion criterion was satisfied. F_N declined with the removal of elements. F_S fluctuated about a value of zero over the entire simulated period.

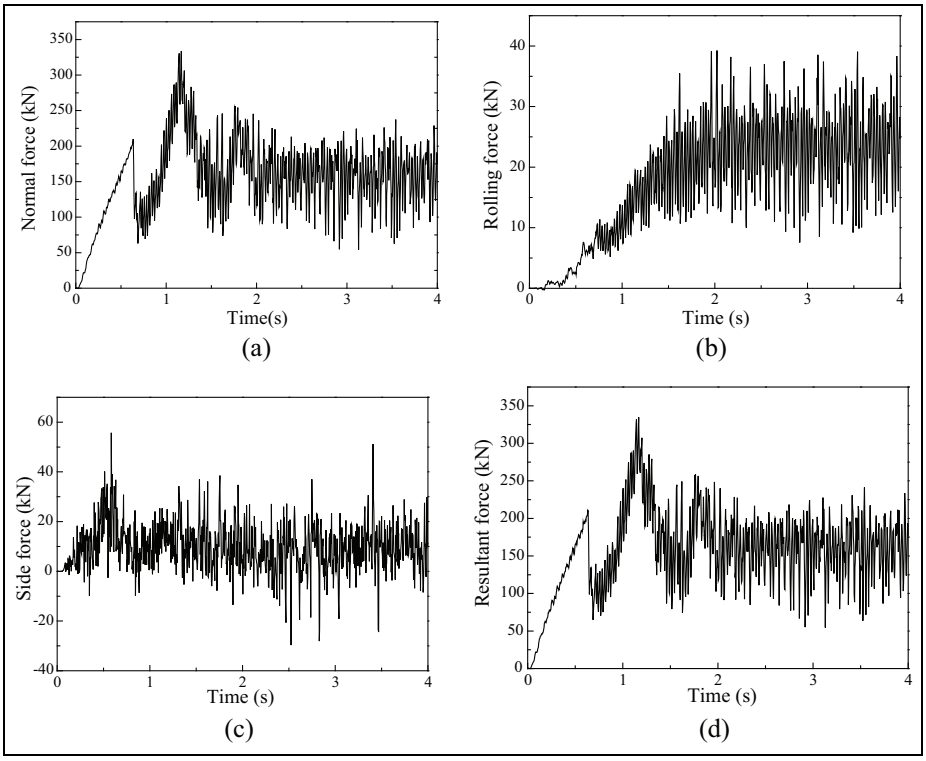

Figure 6. Variation of the forces acting on the disk cutter with respect to time: (a) normal force (F_N) versus time, (b) rolling force (F_R) versus time, (c) side force (F_S) versus time, and (d) resultant force versus time.

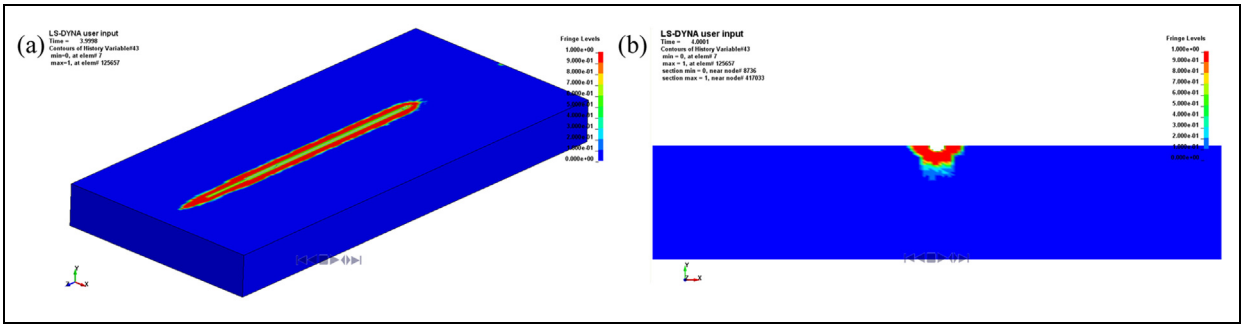

Figure 7. (a) Damage induced in the rock sample and (b) the damage in a cross section normal to the z-axis.

Owing to the nature of the other forces, the resultant force acting on the disk cutter varied in a manner largely equivalent to F_N. Finally, the forces acting on the disk cutter stabilized and fluctuated about their respective average values after the penetration depth reached 7.6 mm (at 2 s), and their average values are given as 160.81 kN (F_N), 18.60 kN (F_R), and 7.71 kN (F_S). The average resultant force is 163 kN.

The forces acting on the disk cutter varied with respect to the penetration depth, and the results of the present simulation are compared with those obtained experimentally from LCM[4] in Figure 8 for penetration depths of 3.8, 5.1, 6.4, and 7.6 mm, respectively. The contact surface area increased with increasing penetration, resulting in correspondingly increased forces. The average values of F_N derived from the simulation are in good agreement with the experiment values, F_R is about 10% of F_N, and the average values of F_N and F_R are slightly smaller than those of the experimental results.

In the process of tunnel excavation, the strength of a compressed brittle rock strongly depends on the lateral confining pressure, where the rock compressive strength increases with increasing confining pressure. The peak stress and corresponding strain also increase. To illustrate the influence of confining pressure on the cutting forces, an equivalent confining pressure was applied to the free surfaces of the rock sample in the simulation at

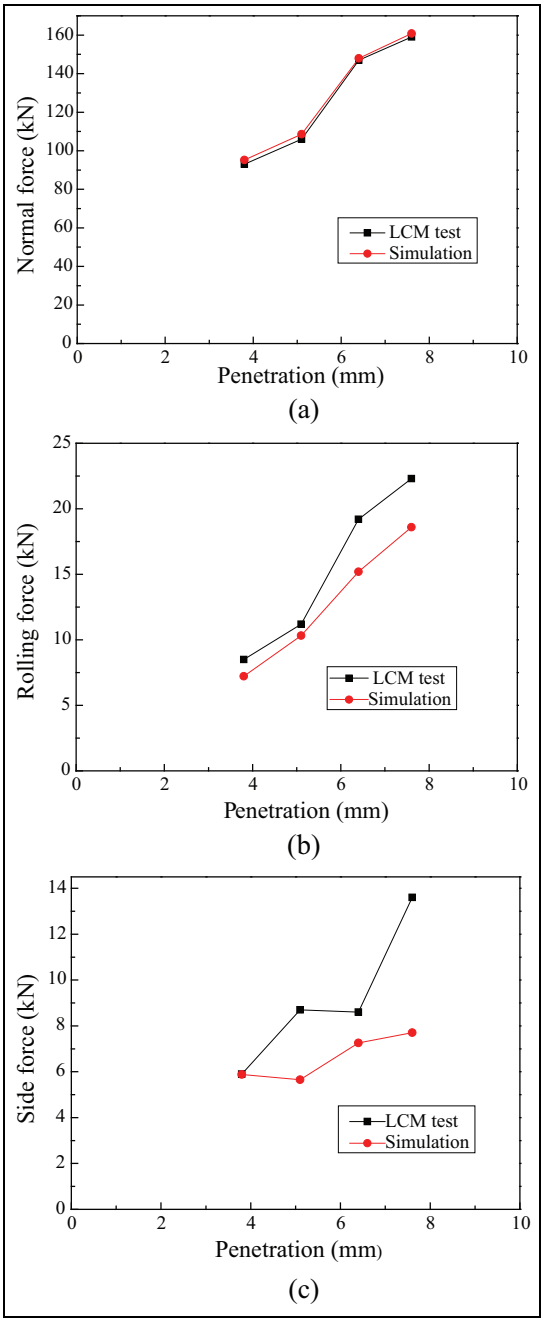

Figure 8. Relationships between the forces acting on the disk cutter and penetration depth, as establish by the present simulations relative to those obtained experimentally from a linear cutting machine:[4] (a) the relationship between normal force (F_N) and penetration depth, (b) the relationship between rolling force (F_R) and penetration depth, and (c) the relationship between side force (F_S) and penetration depth.

a penetration depth of 7.6 mm. The cutter forces obtained by simulation during the cutting process were, respectively, calculated for confining pressures of 10, 15, 20, 25, and 30 MPa, as shown in Figure 9. The values of F_N are noticeably increased when exerting a

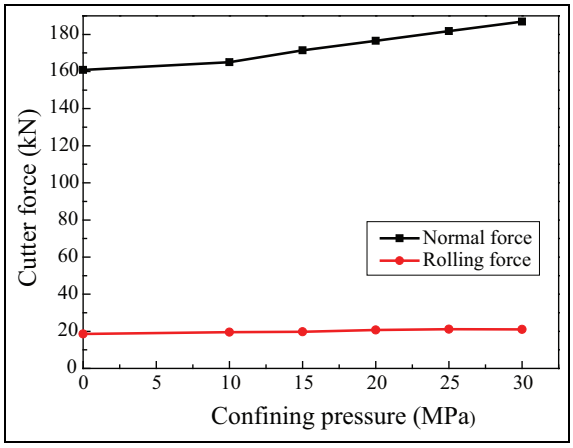

Figure 9. Variations in the normal (F_N) and rolling (F_R) forces with respect to confining pressure.

confining pressure on the rock sample. The confining pressure not only increases the strength of the rock but can also transform the rock from a brittle material to a plastic material, such that F_N becomes greater than that for an unconfined rock surface. However, no obvious change is observed for F_R, indicating that the confining pressure has little influence on it. The value of F_S fluctuated about zero, as shown in Figure 6(c), providing an average value much smaller than the other two force components. Therefore, the effect of confining pressure on this component was not considered.

Another factor that affected the rock strength is the temperature. In the process of tunnel excavation, the surrounding rock mass may experience a certain high temperature. The previous study shows that with the increase in temperature, the brittleness of rock is weakened and the ductility is strengthened. The peak strength is decreased. The cutter forces obtained by simulation were then, respectively, calculated for different temperatures of 25°C, 50°C, 75°C, 100°C, 125°C, and 150°C, as shown in Figure 10. The normal and rolling forces decreased with increasing temperatures. The result is in agreement with the literature.[43]

The rock is a rate-dependent material. Zhang and Zhao[44] described in detail the development and the state of the art in dynamic testing techniques and dynamic mechanical behavior of rock materials. When the strain rates of rock material changed with certain range from 10^{-5} to 10^{1} s^{-1}, there was little variation in the compressive strength. The strain rate of rock sample is in this range during the process of disk cutters breaking rock. So, the cutter forces changed with different strain rates are not simulated.

Rock fragmentation process for two disk cutters

Effect of cutter spacing on the rock fragmentation process. The s/p ratio for two disk cutters is an essential

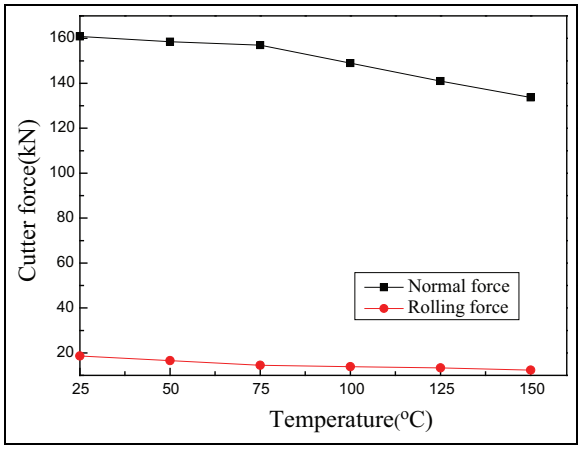

Figure 10. Variations in the normal (F_N) and rolling (F_R) forces with different temperatures.

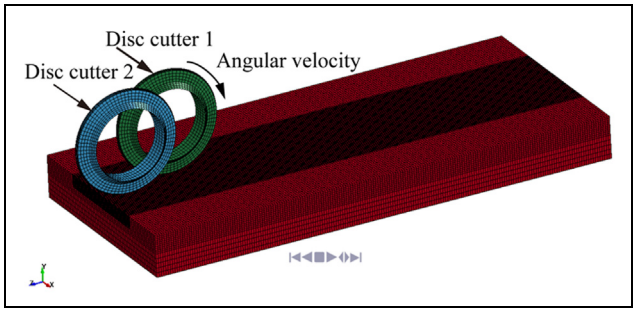

Figure 11. Finite element model of the rock and two disk cutter systems.

parameter in the cutting process, and an optimal value of s/p exists for each specific rock formation. The size of the rock sample employed in this simulation was equivalent to that employed in the previous section, and all other modeling parameters were unchanged. The finite element model employed for simulation of the two disk cutters was establish as shown in Figure 11. We assumed that the two disk cutters were installed in tandem, the first in the front and the second following by 220 mm. The obtained cross-sectional damage contours normal to the z-axis are shown in Figure 12 for the respective cutter spacing values of 51, 76, 100, and 120 mm. The damage area under each disk cutter exhibits a large overlap for a cutter spacing of 51 mm, whereas the damage region is disconnected when the cutter spacing is 120 mm. The red area represents the damage or fracture part of the rock sample. These are the chips during excavating tunnel. Reasonable cutter spacing values based on the simulation results are 76 and 100 mm.

Values of the SE were obtained according to the numerical results with different s/p ratios, as shown in Figure 13, and are used to compare the relative cutting efficiency. A very narrow spacing initially results in a high SE for a given penetration. The value of SE decreases until a relative low level is reached. After that the spacing is further increased followed by an increasing SE. This indicates that the SE is minimal at a particular cutter spacing, and thus, cutting is optimal.[4]

For penetration depths of 7.6 mm, the minimum SE value occurs at an s/p value of 10. The optimum values of s/p varied from 10 to15. For s/p ratios of 15 or

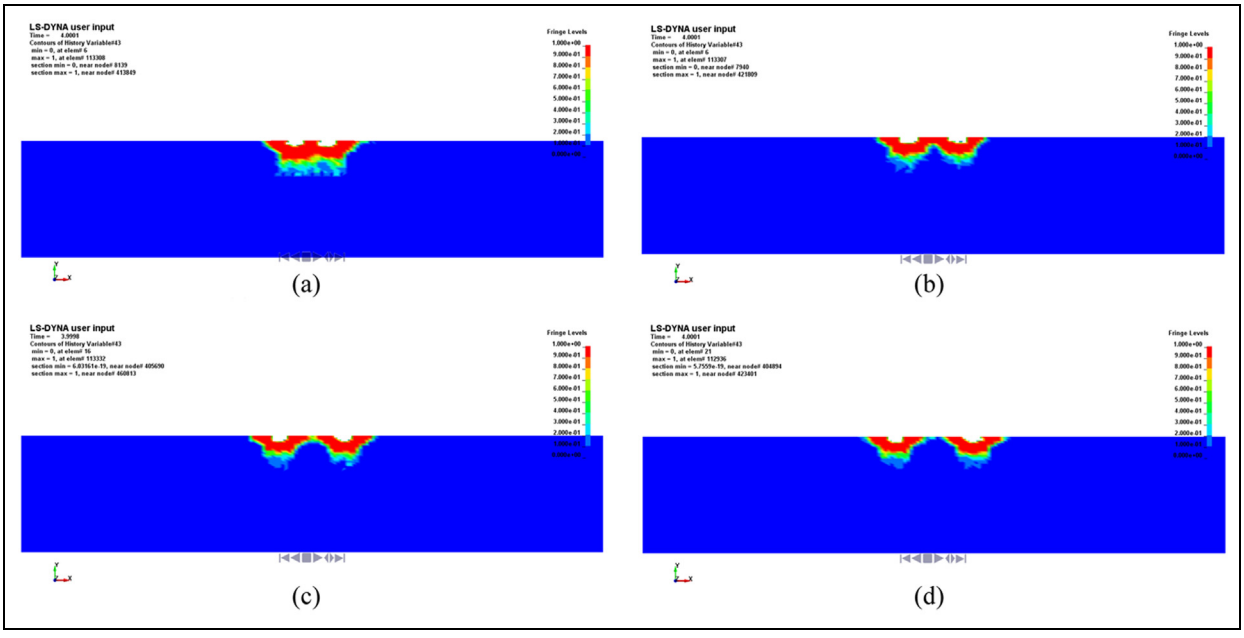

Figure 12. Damage contours normal to the z-axis for different cutter spacing values of (a) 51, (b) 76, (c) 100, and (d) 120 mm.

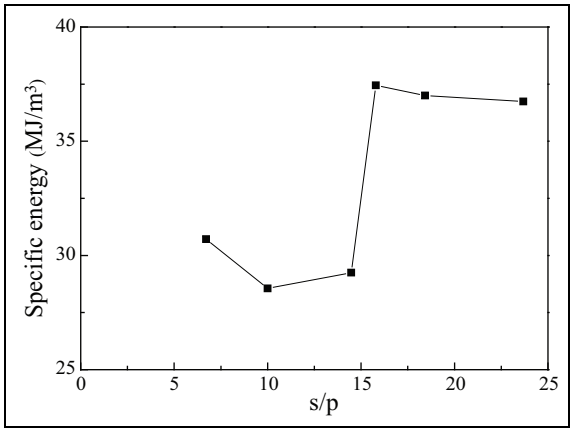

Figure 13. Relationship between the *s*/*p* ratio and the specific energy for the two disk cutters.

greater, the damage region obtained by simulation existing between the cut traces was independent, leading to the formation of ridges. The results obtained from the present numerical modeling agreed well with those obtained during LCM testing.[4]

Forces acting on the two disk cutters. The average values of F_N and F_R acting on the two disk cutters varied with cutter spacing, as shown in Figure 14. The average forces acting on the first cutter are greater than those acting on the second for spacing values of 51 and 76 mm (and, for F_R, 100 mm as well). For F_N, the average values on the two disk cutters differ by 1–3 kN, and the maximum value of which occurred at a cutter spacing of 76 mm. The average values of both F_N and F_R gradually reduced for spacing values greater than 76 mm and remained stable for spacing values of 120 and 140 mm. The different forces acting on the two tandem cutting disks for the more closely spaced configurations are owing to the fact that the first cutter causes some damage to the rock, and the relatively close spacing results in reduced forces acting on the second cutter. However, when the spacing exceeds a critical value, the cutting activities of the two cutters do not interact with each other, and the forces acting on the two cutters are equivalent.

Conclusion

The previous studies are mainly focused on the 2D numerical modeling of the rock fragmentation based on the DEM and the FEM. The presented model was applied to simulate the fracture process with disk cutters by 3D FEM. A plastic damage material model for rock based on the extended Drucker–Prager strength criterion and the Johnson–Cook material model was proposed to describe the plastic compressive damage of

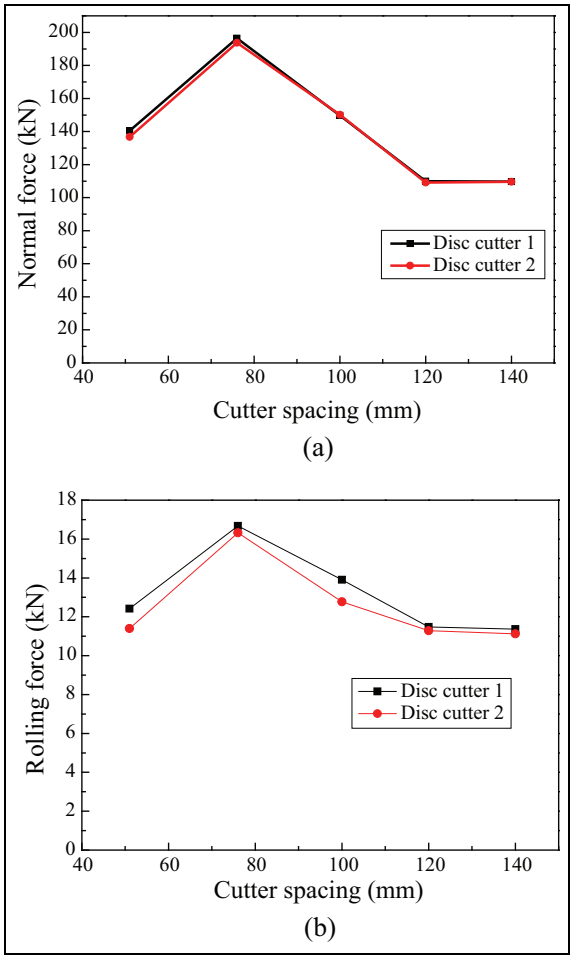

Figure 14. Force variations with respect to cutter spacing: (a) average normal force (F_N) with cutter spacing and (b) average rolling force (F_R) with cutter spacing.

rock-like material. The model was implemented into finite element software LS-DYNA. A finite element model comprising rock and a disk cutter was established to simulate the rock-cutting process. The presented model was applied to simulate the rock fracture process with disk cutters. The damage region of rock and cutting forces were obtained. The results accurately reflected the damage and failure process of rock and were in good agreement with LCM test results.

According to the simulation results, both the normal and the rolling forces fluctuated about average values that increased with increasing penetration depth. The side force fluctuated about a value of zero, which changed little with increasing penetration depth. The normal force exhibited an obvious increase under conditions of an applied confining pressure, whereas no significant change in the rolling force was observed.

The optimum *s*/*p* values determined during numerical modeling of two disk cutter systems agree well with those obtained during LCM testing. The optimum *s*/*p*

values varied from 10 to 15. For s/p ratios of 15 or greater, the damage area existing between cut traces did not overlap, leading to the formation of ridges. The average normal and rolling forces acting on the first cutter are slightly greater than those acting on the second when the cutter spacing was relatively small.

Declaration of conflicting interests

The author(s) declared no potential conflicts of interest with respect to the research, authorship, and/or publication of this article.

Funding

The author(s) disclosed receipt of the following financial support for the research, authorship, and/or publication of this article: This work was financially supported by the National Basic Research Program of China under grant no. 2013CB035402.

References

1. Cho JW, Jeon S, Yu SH, et al. Optimum spacing of TBM disc cutters: a numerical simulation using the three-dimensional dynamic fracturing method. *Tunn Undergr Sp Tech* 2010; 25: 230–244.
2. Chang SH, Choi SW, Bae GJ, et al. Performance prediction of TBM disc cutting on granitic rock by the linear cutting test. *Tunn Undergr Sp Tech* 2006; 21: 271.
3. Rostami J, Ozdemir L and Nilsen B. Comparison between CMS and NTH hard rock TBM performance prediction models. In: *Proceedings of the annual technical meeting of the Institute of Shaft Drilling and Technology (ISDT)*, Las Vegas, NV, 1996, pp.1–11, http://emi.mines.edu/UserFiles/File/earthMechanics/tbm/tbm1.pdf
4. Gertsch R, Gertsch L and Rostami J. Disc cutting tests in Colorado Red Granite: implications for TBM performance prediction. *Int J Rock Mech Min Sci* 2007; 44: 238–246.
5. Cho JW, Jeon S, Jeong HY, et al. Evaluation of cutting efficiency during TBM disc cutter excavation within a Korean granitic rock using linear-cutting-machine testing and photogrammetric measurement. *Tunn Undergr Sp Tech* 2013; 35: 37–54.
6. Rostami J and Ozdemir L. A new model for performance prediction of hard rock TBM. In: Bowerman LD and Monsees JE (eds) *Proceedings of the rapid excavation and tunnelling conference*. Boston, MA: AIME, 1993, pp.793–809.
7. Bruland A. *Hard rock tunnel boring*. PhD Thesis, Norwegian University of Science and Technology (NTNU), Trondheim, 1998.
8. Evans I. A theory of the basic mechanics of coal ploughing. In: Clark GB (ed.) *Proceedings of the international symposium on mining research*, vol. 2. London: Pergamon Press, 1962, pp.761–798.
9. Nishimatsu Y. The mechanics of rock cutting. *Int J Rock Mech Min Sci Geomech Abstr* 1972; 9: 261–270.
10. Roxborough FF and Phillips HR. Rock excavation by disc cutter. *Int J Rock Mech Min Sci Geomech Abstr* 1975; 12: 361–366.
11. Ozdemir L, Miller R and Wang FD. *Mechanical tunnel boring prediction and machine design*. Final project report to NSF APR73-07776-A03. Golden, CO: Colorado School of Mines, 1978.
12. Sanio HP. Prediction of the performance of disc cutters in anisotropic rock. *Int J Rock Mech Min Sci Geomech Abstr* 1985; 22: 153–161.
13. Hassanpour J, Rostami J and Zhao J. A new hard rock TBM performance prediction model for project planning. *Tunn Undergr Sp Tech* 2011; 26: 595–603.
14. Barton N. *TBM tunnelling in jointed and faulted rock*. Rotterdam: Balkema, 2000.
15. Yagiz S. Utilizing rock mass properties for predicting TBM performance in hard rock condition. *Tunn Undergr Sp Tech* 2008; 3: 326–339.
16. Zhao Z, Gong QM, Zhang Y, et al. Prediction model of tunnel boring machine performance by ensemble neural networks. *Geomech Geoengin* 2007; 2: 123–128.
17. Menezes PL, Lovell MR, Avdeev IV, et al. Study on the formation of discontinuous chips during rock cutting using an explicit finite element model. *Int J Adv Manuf Tech* 2014; 70: 635–648.
18. Park KI, Chang SH, Choi SW, et al. Prediction of the optimum cutting condition of TBM disc cutter in Korean granite by the linear cutting test. In: *Proceedings of the Korean Society for Rock Mechanics conference*, Seoul, Korea, March 2006, pp.217–236. Seoul, Korea: Korean Society for Rock Mechanics.
19. Innaurato N, Oggeri C, Oreste PP, et al. Experimental and numerical studies on rock breaking with TBM tools under high stress confinement. *Rock Mech Rock Eng* 2007; 40: 429–451.
20. Tulu IB and Heasley KA. Calibration of 3D cutter-rock model with single cutter tests. In: *The 43th U.S. rock mechanics symposium & 4th U.S.–Canada rock mechanics symposium*, Asheville, NC, 28 June–1 July 2009. Alexandria, VA: American Rock Mechanics Association (ARMA).
21. Tan XC, Kou SQ and Lindqvist PA. Application of the DDM and fracture mechanics models on the simulation of rock breakage by mechanical tools. *Eng Geol* 1998; 49: 277–284.
22. Jing L. A review of techniques, advances and outstanding issues in numerical modelling for rock mechanics and rock engineering. *Int J Rock Mech Min Sci* 2003; 40: 283–353.
23. Gong QM, Zhao J and Jiao YY. Numerical modeling of the effects of joint orientation on rock fragmentation by TBM cutters. *Tunn Undergr Sp Tech* 2005; 20: 183–191.
24. Gong QM, Jiao YY and Zhao J. Numerical modelling of the effects of joint spacing on rock fragmentation by TBM cutters. *Tunn Undergr Sp Tech* 2006; 21: 46–55.
25. Gong QM, Zhao J and Hefny AM. Numerical simulation of rock fragmentation process induced by two TBM cutters and cutter spacing optimization. *Tunn Undergr Sp Tech* 2006; 21: 263.

26. Gong QM and Zhao J. Development of a rock mass characteristics model for TBM penetration rate prediction. *Int J Rock Mech Min Sci* 2009; 46: 8–18.
27. Rojek J. Discrete element modeling of rock cutting. *Comp Method Mater Sci* 2007; 7: 224–230.
28. Rojek J, Oñate E, Labra C, et al. Discrete element simulation of rock cutting. *Int J Rock Mech Mining Sci* 2011; 48: 996–1010.
29. Moon T and Oh J. A study of optimal rock-cutting conditions for hard rock TBM using the discrete element method. *Rock Mech Rock Eng* 2012; 45: 837–849.
30. Su O and Akcin NA. Numerical simulation of rock cutting using the discrete element method. *Int J Rock Mech Min Sci* 2011; 48: 434–442.
31. Mendoza Rizo JA. *Considerations for discrete element modeling of rock cutting*. PhD Thesis, University of Pittsburgh, Pittsburgh, PA, 2013.
32. Huang H, Lecampion B and Detournay E. Discrete element modeling of tool-rock interaction I: rock cutting. *Int J Numer Anal Met* 2013; 37: 1913–1929.
33. Huang H and Detournay E. Discrete element modeling of tool-rock interaction II: rock indentation. *Int J Numer Anal Met* 2013; 37: 1930–1947.
34. Tang C. Numerical simulation of progressive failure and associated seismicity. *Int J Rock Mech Min Sci* 1997; 34: 249–261.
35. Tang CA, Fu YF, Kou SQ, et al. Numerical simulation of loading inhomogeneous rocks. *Int J Rock Mech Min Sci* 1998; 35: 1001–1007.
36. Liu HY, Kou SQ, Lindqvist PA, et al. Numerical simulation of the rock fragmentation process induced by indenters. *Int J Rock Mech Min Sci* 2002; 39: 491–505.
37. Yu B. *Numerical simulation of continuous minor rock cutting process*. PhD Thesis, College of Engineering and Mineral Resources, West Virginia University, Morgantown, WV, 2005.
38. Jaime MC. *Numerical modeling of rock cutting and its associated fragmentation process using the finite element method*. PhD Thesis, University of Pittsburgh, Pittsburgh, PA, 2010.
39. Johnson GJ and Cook WH. A constitutive model and data for metals subjected to large strains, high strain rates and high temperatures. In: *Proceedings of the seventh international symposium on ballistics*, The Hague, 1983, pp.541–547, http://www.lajss.org/HistoricalArticles/A%20constitutive%20model%20and%20data%20for%20metals.pdf
40. Hibbitt, Karlsson and Sorensen, Inc. *ABAQUS analysis user's manual help online*. Providence, RI: SIMULIA, 2005.
41. Holmquist TJ, Johnson GR and Cook WH. A computational constitutive model for concrete subjected to large strains, high strain rates, and high pressures. In: *Proceedings of 14th international symposium on ballistics*, Quebec City, QC, Canada, 26–29 September 1993, pp.591–600. Quebec: American Defense Prepareness Association.
42. Balci C. Correlation of rock cutting tests with field performance of a TBM in a highly fractured rock formation: a case study in Kozyatagi-Kadikoy metro tunnel, Turkey. *Tunn Undergr Sp Tech* 2009; 24: 423–435.
43. Zhang G, Tan Q, Xia Y, et al. Influence of different rock temperature on rock breaking characteristics of disc cutter tunneling parameters. *J Hunan Univ Nat Sci* 2015; 4: 40–47.
44. Zhang QB and Zhao J. A review of dynamic experimental techniques and mechanical behavior of rock materials. *Rock Mech Rock Eng* 2014; 47: 1411–1478.